ADVANCED MATERIALS INTERFACES
Open Access
www.advmatinterfaces.de

Molecular Templates on Surfaces by Exploiting Supramolecular Chemistry in Langmuir–Blodgett Monolayers

Enrique Escorihuela, Alberto Concellón, Teresa Cardona, Giampaolo Zuccheri, Santiago Martín, José L. Serrano, and Pilar Cea**

Attaining precise control over molecular arrangements is of paramount importance for numerous applications in nanotechnology, particularly in constructing molecular templates to accurately immobilize target materials on surfaces. A strategic combination of supramolecular and interfacial chemistry may serve to build a well-organized molecular network, enabling the subsequent location of target molecules on specific positions of a surface. A supramolecular complex (compound 1) comprised of a melamine unit forming hydrogen bonds with dendritic arms terminated in a coumarin unit is utilized, which readily undergoes photodimerization. The research demonstrates the formation of well-organized Langmuir films of compound 1 which can be transferred on substrates at low surface pressures adopting a lying-flat orientation. Upon irradiation of the pristine films at 365 nm the coumarin units undergo photo-cross linking, leading to the formation of a compact photo-crosslinked film. Incubation of these photo-crosslinked films in a solution containing 1-hexanethiol results in the withdrawal of the melamine and the chemisorption of two thiol molecules per each melamine unit. The nanopores created by the removal of the melamine core are attributed to the disruption of hydrogen bonds in compound 1 by the thiols. This precisely defined molecular network holds significant promise as a template for orchestrating the arrangement of functional materials on surfaces.

1. Introduction

Exquisite control over porous materials, 2D nano-porous membranes, well-ordered mono and multi-layered films, as well as 2D systems and interfaces, stands as an essential tool in contemporary nanofabrication. This level of control reached by nanoarchitectonic tools finds extensive applications across various domains, spanning from the production of (bio)sensors to the capture and containment of greenhouse gases, extending its influence into DNA sequencing, nanoreactors, photovoltaic and thermoelectric cells, as well as nanoelectronics, spintronics, quantum computing, molecular (thermo)electronic devices, among a plethora of others.[1–17]

For these reasons, the assembly of thin templates on surfaces has gained significant attention due to its key role in directing the organization of functional materials, opening the path toward the

E. Escorihuela, T. Cardona, S. Martín, P. Cea
Departamento de Química Física
Facultad de Ciencias
Universidad de Zaragoza
Zaragoza 50009, Spain
E-mail: pilarcea@unizar.es

E. Escorihuela, A. Concellón, T. Cardona, S. Martín, J. L. Serrano, P. Cea
Instituto de Nanociencia y Materiales de Aragón (INMA)
CSIC-Universidad de Zaragoza
Zaragoza 50009, Spain
E-mail: joseluis@unizar.es

The ORCID identification number(s) for the author(s) of this article can be found under https://doi.org/10.1002/admi.202301090

DOI: 10.1002/admi.202301090

E. Escorihuela, S. Martín, P. Cea
Laboratorio de Microscopias Avanzadas (LMA)
Universidad de Zaragoza
Zaragoza 50018, Spain

A. Concellón, J. L. Serrano
Departamento de Química Orgánica
Facultad de Ciencias
Universidad de Zaragoza
Zaragoza 50009, Spain

G. Zuccheri
Department of Pharmacy and Biotechnology and Interdepartmental Center for Industrial Research on Life Science and Health Technologies at the Alma Mater Studiorum Università di Bologna, and S3 Center of the Institute of Nanoscience of the National Research Council
Bologna 40127, Italy

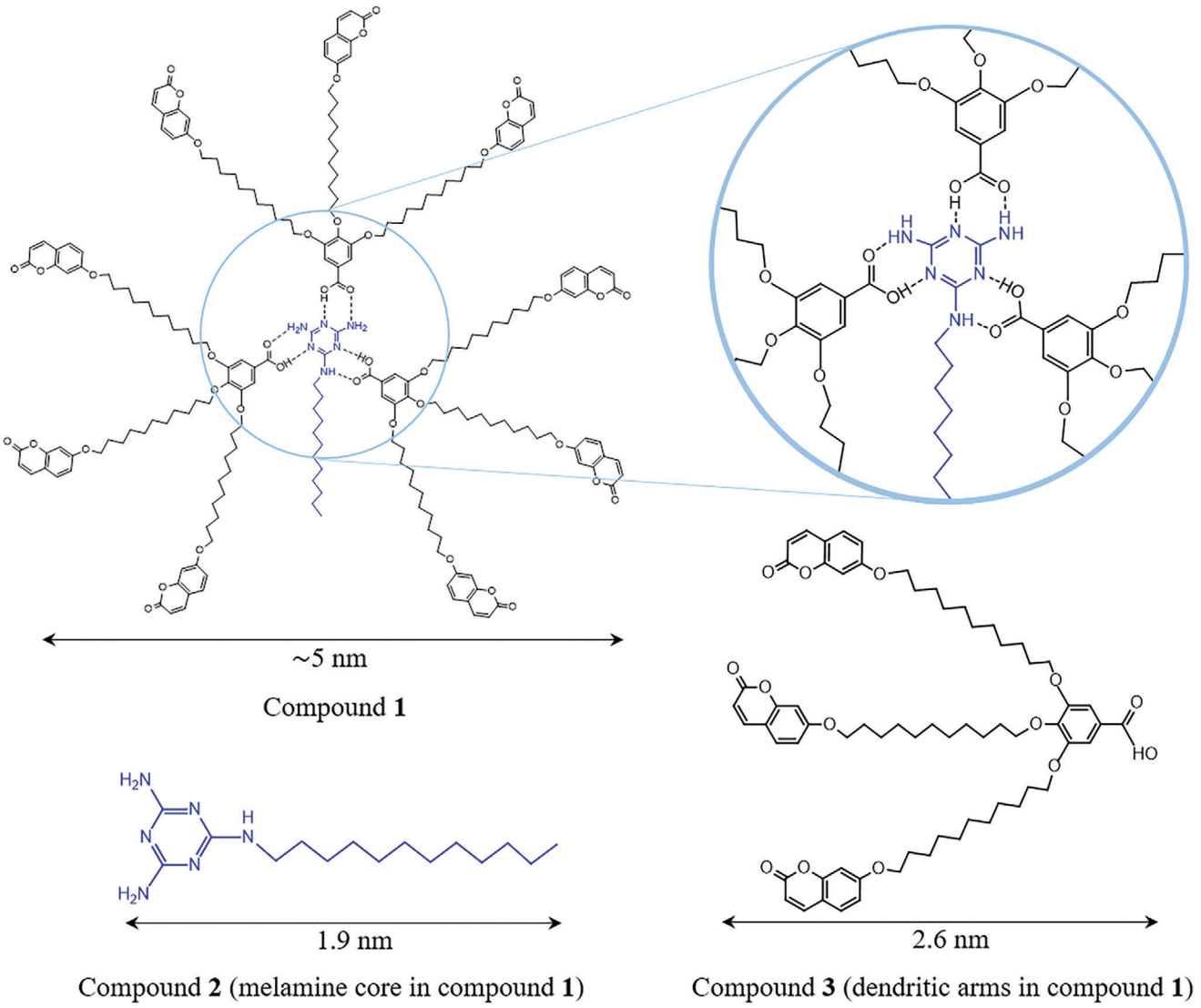

Figure 1. Chemical structure of compounds **1**,**2**, and **3**.

fabrication of assemblies that integrate a precise number of molecules in specific locations or even arrays of unimolecular devices. While molecular networks have been reported previously in the literature, initially their preparation often required methodologies involving the sublimation of the molecular material within high vacuum systems.[18] Despite the high quality of these networks, the restricted vacuum fabrication conditions, together with the fact that structures produced through this process do not always withstand removal from the vacuum chamber represent significant drawbacks. In response to these limitations, other methods have been developed including creation of nanopores by irradiating thin layers of a material with a focused high-energy electron beam,[12,19] but this is an expensive and challenging-to-scale process. As an alternative to these technologies, solution-based methods have been developed more recently. These methods rely on self-assembly processes governed by molecular interactions such as hydrogen bonding,[20] dipolar coupling,[21] alkyl chain interdigitation,[22] or metal–ligand coordination.[23] Recent advancements have witnessed the emergence of Langmuir-Blodgett (LB) and Langmuir–Schaefer (LS) methodologies for preparing molecular networks and molecular templates.[11,16] The Langmuir technique is a powerful methodology for the organization of organic materials at the air-water interface. These monolayers can be precisely transferred onto solid supports at specific target surface pressures, thus yielding highly ordered LB/LS mono or multilayers.

In this context, we recently reported Langmuir-Blodgett monolayers incorporating a zinc-metallated porphyrin onto a gold substrate.[24] Subsequently, we integrated a functionalized molecular wire at the Zn position of the porphyrin derivative, resulting in the fabrication of unimolecular electronic devices due to the coupling between Zn and the amine-terminal group of the molecule. Expanding upon this prior research, we introduce here a novel advancement: the fabrication of an openable monolayer network featuring a supramolecular complex, designated here as compound **1**. As depicted in **Figure 1**, complex **1** is formed by

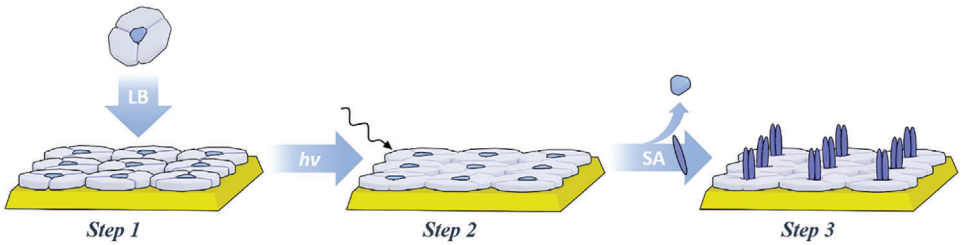

Scheme 1. Cartoon showing (*step 1*) the fabrication of an LB monolayer onto a solid support followed by (*step 2*) the photodimerization of the coumarin units and by (*step 3*) the withdrawal of the melamine units with creation of in-plane nanopores and the entrance of thiol-terminated molecules onto the nanopores that are self-assembled onto the bottom substrate. Note that the orientation of the thiol molecules depicted here is for visualization purposes only. Depending on the specific molecule used to fill the nanopores, an investigation of the orientation of this material should be conducted. Alternatively, if desired the precise orientation of the molecules filling the nanopore could be defined using engineered molecular synthesis approaches.

a melamine derivative (N^2-dodecyl-1,3,5-triazine-2,4,6-triamine) (compound **2**), which acts as a template core, hydrogen-bonded to three dendrons derived from a 3,4,5-triundeciloxycarboxilic acid incorporating photodimerizable coumarin moieties in the terminal positions of the chains (compound **3**). Melamine has been functionalized with a dodecyloxy chain to promote its solubility in the complex formation process.

We reported before[25] that hydrogen-bonded complex **1** facilitates the production of columnar hexagonal liquid crystal arrangements in bulk, leading to the creation of nanoporous polymers with size- and charge-selective adsorption capabilities. In this contribution, we demonstrate the topologically controlled placement on a gold surface of thiol-terminated (bio)organic materials (see **Scheme 1**). In the first step, a pristine monolayer incorporating compound **1** is immobilized on a gold surface, using the Langmuir-Blodgett technique. In the second step, the monolayer is stabilized by photodimerization of the coumarin units, obtaining a photo-crosslinked plastic film. Finally, the hydrogen bonds retaining the melamine unit are broken by exposing the photo-crosslinked film to a solution of 1-hexanethiol (compound **4**) in ethanol. In this step, two thiol-terminated molecules enter into the nanopore created by the removal of the melamine unit and self-assemble on the underlying gold surface. This approach allows precise placement of thiol-terminated molecules into the molecular network using self-assembly methodologies (Scheme 1).

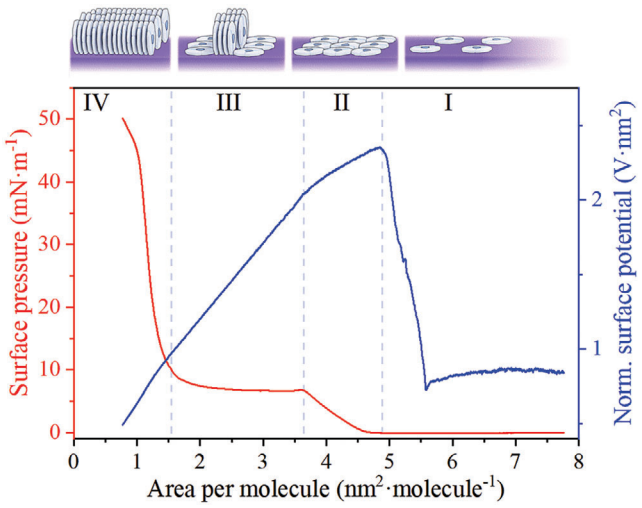

Figure 2. Surface pressure (red) and normalized surface potential (blue) isotherms for compound **1** at the air–water interface. The top cartoon indicates the organization of compound **1** in each of the phases and phase transitions in the isotherms as discussed in the text.

2. Results and Discussion

Figure 2 shows a surface pressure vs. area per molecule, π-*A*, isotherm for compound **1**, together with the normalized surface potential vs. area per molecule, Δ*Vn*-*A*, isotherm. These isotherms are highly reproducible (see the details for the experimental conditions in the Supporting Information, Section 1, as well as a comprehensive discussion and interpretation of the isotherms). Despite the reproducibility of the isotherms, a concern that raised our minds is whether the supramolecular structure of compound **1** could be broken when it is spread at the air-water interface by a competition in the formation of hydrogen bonds with water. In order to confirm or rule out the rupture of the supramolecular structure, isotherms of compound **2**, **3** and their mixtures in the (1:1), (1:2), and (1:3) ratios were obtained and compared with the isotherm of **1** (Figure S2, Supporting Information). From these isotherms, we concluded that the supramolecular structure of compound **1**, remains intact following its dispersion on the water surface (see full discussion in Section 1.3 in the Supporting Information).

A thorough investigation of the Langmuir films of compound **1** was conducted, encompassing an analysis not only of surface pressure and surface potential isotherms but also of compression modulus, hysteresis experiments, Brewster angle microscopy, and UV–vis reflection spectroscopy, as detailed in the Supporting Information. From this study, we conclude that at surface pressures below the plateau in the isotherm, compound **1** is arranged in a quasi-flat orientation on the water surface. However, the presence of the plateau signifies a phase transition, with the molecules adopting a more vertical orientation, as depicted in the illustrative cartoon in Figure 2.

Monolayers of compound **1** were transferred onto solid supports using the Langmuir–Blodgett method, both before and after the plateau in the isotherm, at surface pressures of 4 and 27 mN m^{-1}, respectively, for comparative analysis. The surface coverage of the pristine transferred films, Γ, was determined using a quartz crystal microbalance (QCM). The surface coverages

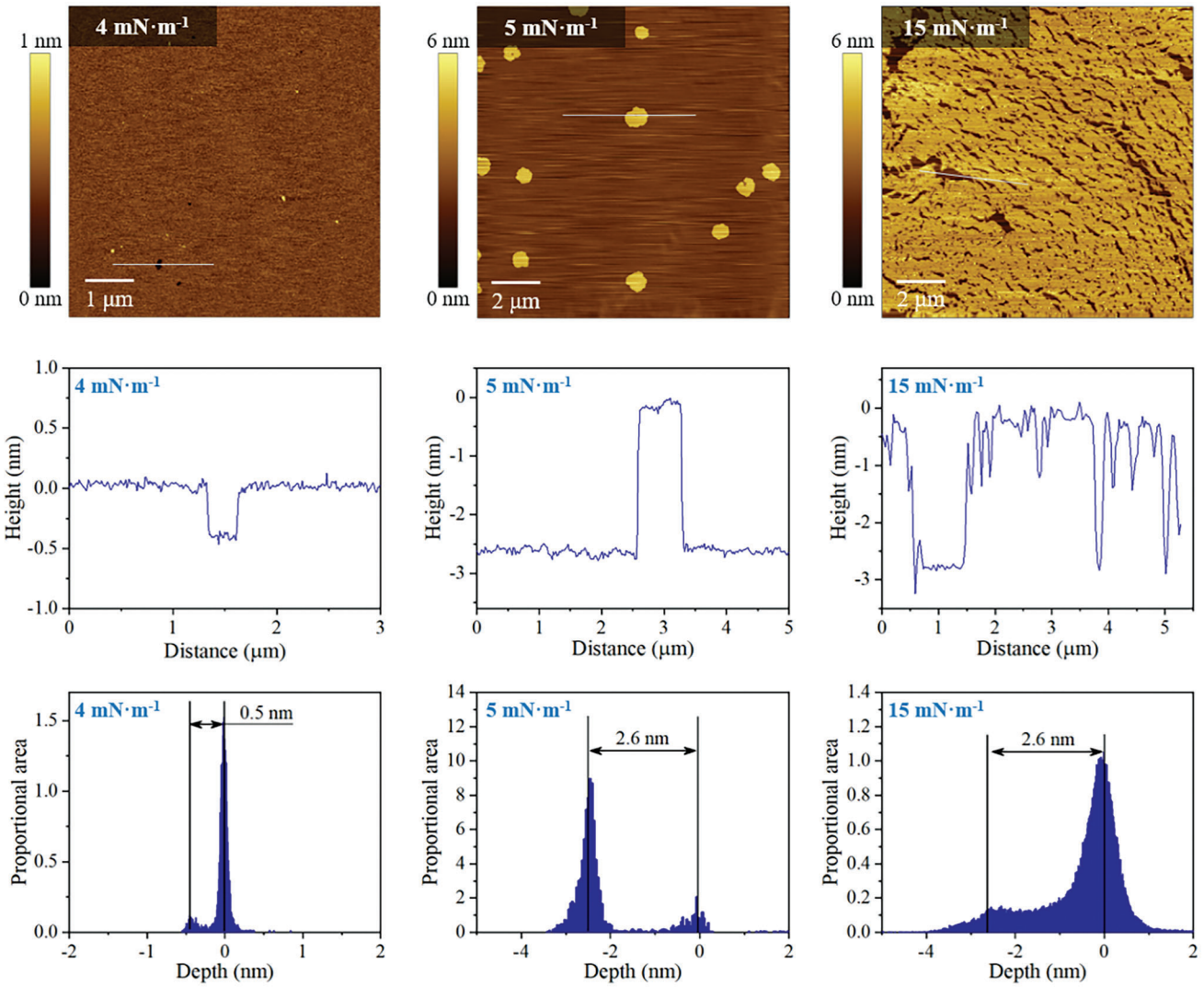

Figure 3. Top panel: AFM images of one-layer pristine LB films of compound **1** transferred at 4,5, and 15 mN m^{-1} onto a mica substrate. Bottom panel: height profile (—) and thickness analysis for each of the studied samples above.

measured were 3.4×10^{-11} and 1.5×10^{-10} mol cm^{-2} at surface pressures of 4 and 27 mN m^{-1}, respectively (for further details, refer to Section 2 in the Supporting Information). These results are in good agreement with the surface coverage for a Langmuir film at each of these two target surface pressures of transference, which were 4.2×10^{-11} and 1.4×10^{-10} mol cm^{-2}, respectively.

Atomic Force Microscopy was used to examine the morphology of the obtained films. Pristine LB monolayers transferred at surface pressures below the plateau in the isotherm (e.g. 4 mN m^{-1}) exhibit a very homogenous morphology, as shown in **Figure 3**, characterized by a lack of 3D structures and a thickness of ≈ 0.5 nm. Figure 3 displays a representative AFM image, while Figure S11 (Supporting Information) provides the topography of a bare mica AFM image for comparison purposes. Moreover, Figure S12 (Supporting Information) depicts an AFM area for a film transferred at 4 mN m^{-1} exhibiting some defects that allow for the estimation of the film thickness. Additionally, the thickness of LB films transferred at a target pressure of 4 mN m^{-1} was determined by utilizing the attenuation of the gold signal, Au 4f, in a film transferred onto a gold substrate (refer to Supporting Information, Section 2.5). The result yields a thickness value of 0.55 ± 0.05 nm. These experimental thickness values for the transferred films are in good agreement with the arrangement of compound **1** in an almost flat orientation, parallel to the surface. At a surface pressure of 5 mN m^{-1} (beginning of the plateau in the isotherm, Figure 2), AFM images reveal a few higher structures within an otherwise uniform pristine film. These structures feature a thickness of 2.6 nm, suggesting a configuration where compound **1** is oriented in a more perpendicular manner with respect to the substrate. Pristine films transferred after the plateau in the isotherm (i.e., 15 mN m^{-1}) are relatively homogeneous, primarily characterized by a thickness of 2.6 nm, with some less covered regions tentatively attributed to uncovered regions or areas where molecules remain in a relatively flat orientation. Pristine films transferred at even higher surface pressures, 27 mN m^{-1}, display a similar topography to those transferred at 15 mN m^{-1}

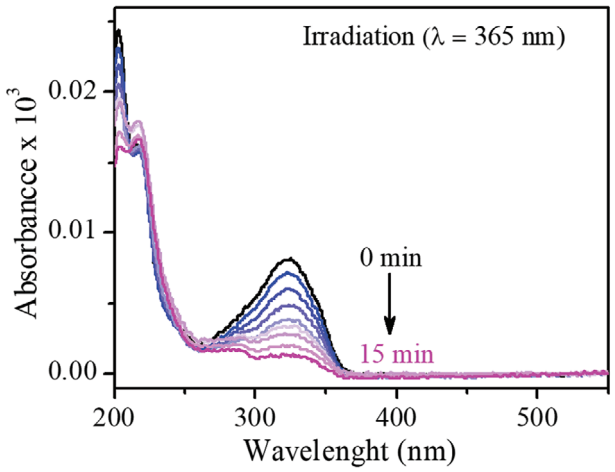

Figure 4. UV–vis spectra of a one-layer LB film of compound **1** on quartz before and after the photodimerization process induced by irradiation with light at 365 nm, transitioning from the unirradiated film (— black) to the film irradiated for 15 min (— pink).

but show a higher surface coverage (Figure S13, Supporting Information).

Taking into account the capabilities of compound **1** to act as a molecular template by removal of the melamine unit, we aim to build upon our previous contributions in bulk[25] by exploiting the immobilization of compound **1** on surfaces. Specifically, we focus on films transferred below the plateau in the isotherm, where the melamine unit is exposed on the surface (flat orientation of compound **1**) and can be potentially removed under suitable conditions. For these reasons, pristine LB films transferred at a surface pressure of 4 mN m^{-1} onto mica and gold-on-mica substrates were photo-crosslinked using 365 nm light. This photo-crosslinking process was monitored using UV–vis spectroscopy (**Figure 4**).

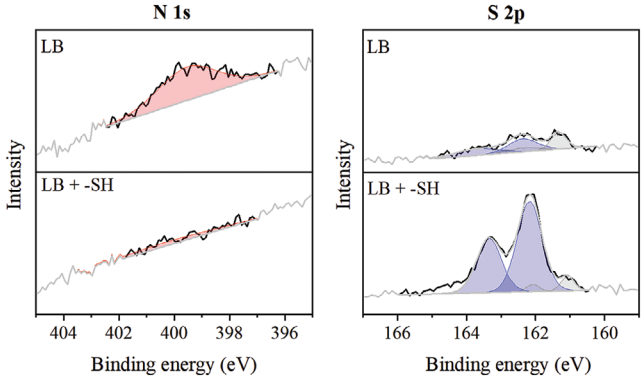

Figure 5. Left: XPS spectra in the N1s region corresponding to (top panel) the photo-crosslinked one-layer LB film of compound **1** onto a gold-on-mica substrate and (bottom panel) the same layer after incubation in a solution of compound **4** in ethanol for 1 h. Right: XPS spectra in the S2p region corresponding to (top panel) the pristine 1-layer LB film of compound **1** and (bottom panel) the same layer after incubation in a solution of compound **4** in ethanol for 1 h. The broadband in the N1s corresponds to the two types of N atoms in compound **1**, that is, = N- and –NH- without any deconvolution treatment.

Subsequent AFM analysis demonstrated the resulting photo-crosslinked films to be highly homogeneous (Section 2.2, Supporting Information). Importantly, the photo-crosslinked LB films maintain their structure after immersion in ethanol, in contrast with the pristine films (see Section 2.6, Supporting Information). In addition, these photo-crosslinked films exhibit remarkable stability, as we have examined films (using AFM and UV–vis spectroscopy) fabricated several months apart and found that their integrity remained unchanged. As previously outlined in the introduction section, the main goal of this work is to arrange compound **1** in a flat monolayer, from which the melamine unit can be selectively removed to create nanoporous monolayers. This approach allows for the precise positioning of specific materials on the surface, presenting potential applications such as the formation of extensive arrays of single-molecule functional units for sensing, biosensing, and electronic applications, among others, as illustrated in Scheme 1. After immersion of a monolayer of compound **1** into a 10^{-3} M solution of 1-hexanethiol (compound **4**) in ethanol, the XPS spectrum of the photo-crosslinked LB films revealed a complete removal of the melamine unit (disappearance of the nitrogen peak at 399.4 eV that is observed for the powder of compound **1**), and the subsequent insertion of the thiol compound (**Figure 5**). The XPS spectrum of photo-crosslinked LB films in the S2p region shows a doublet peak, S2p3/2 and S2p1/2, due to the spin-orbit splitting effect[26] at 162.1 and 163.3 eV, respectively, featuring a peak separation of 1.2 eV and an area ratio of 2:1. These peaks are associated with the thiol group being chemisorbed on the gold substrate,[27,28] with free –SH peaks associated to higher energies.[29] The remaining weak signals in the S2p region are attributed to adventitious sulfur bound to gold, unrelated to compound **4**, as they also appear in untreated LB film samples. These observations (removal of the melamine unit and entrance of thiols in the nanopores) were also confirmed by UV–vis spectroscopy (Figure S18, Supporting Information), with a decrease in the band at 219 nm (attributable to the melamine but also to the aromatic groups in the dendritic units), and preservation of the bands corresponding to the photodimerized coumarin.

^{13}C-NMR spectra in CD_2Cl_2 solution, **Figure 6**, undoubtedly demonstrate that, after the addition of 1-hexanethiol to a CD_2Cl_2 solution of compound **1** in a 5:1 molar ratio, the carbon atoms involved in the hydrogen bonds between compound **2** and compound **3** (or those close to them) shift to the free form (i.e., the hydrogen bonds are weakened by the addition of the 1-hexanethiol). Specifically, the ^{13}C (C_β) signals of the core compound **2** shift from 164.73 to 166.04 ppm after the addition of 1-hexanethiol (note that C_β of free **2** appears at 167.39 ppm). Moreover, the ^{13}C signals of the carboxylic group of compound **3** (C_S) experience a downfield displacement of +0.41 ppm after the addition of the thiol, indicating weakened hydrogen bonds between compound **2** and compound **3**. Besides, it is particularly noteworthy that the carbons close to the hydrogen bonds (e.g., C_R and C_Q) also experience slight displacements, further proving the weakening of the hydrogen bonds after the addition of compound **4**. Table S1 (Supporting Information) in Section 3.1 of the Supporting Information provides full details about shift variations of the main carbon signals involved, and

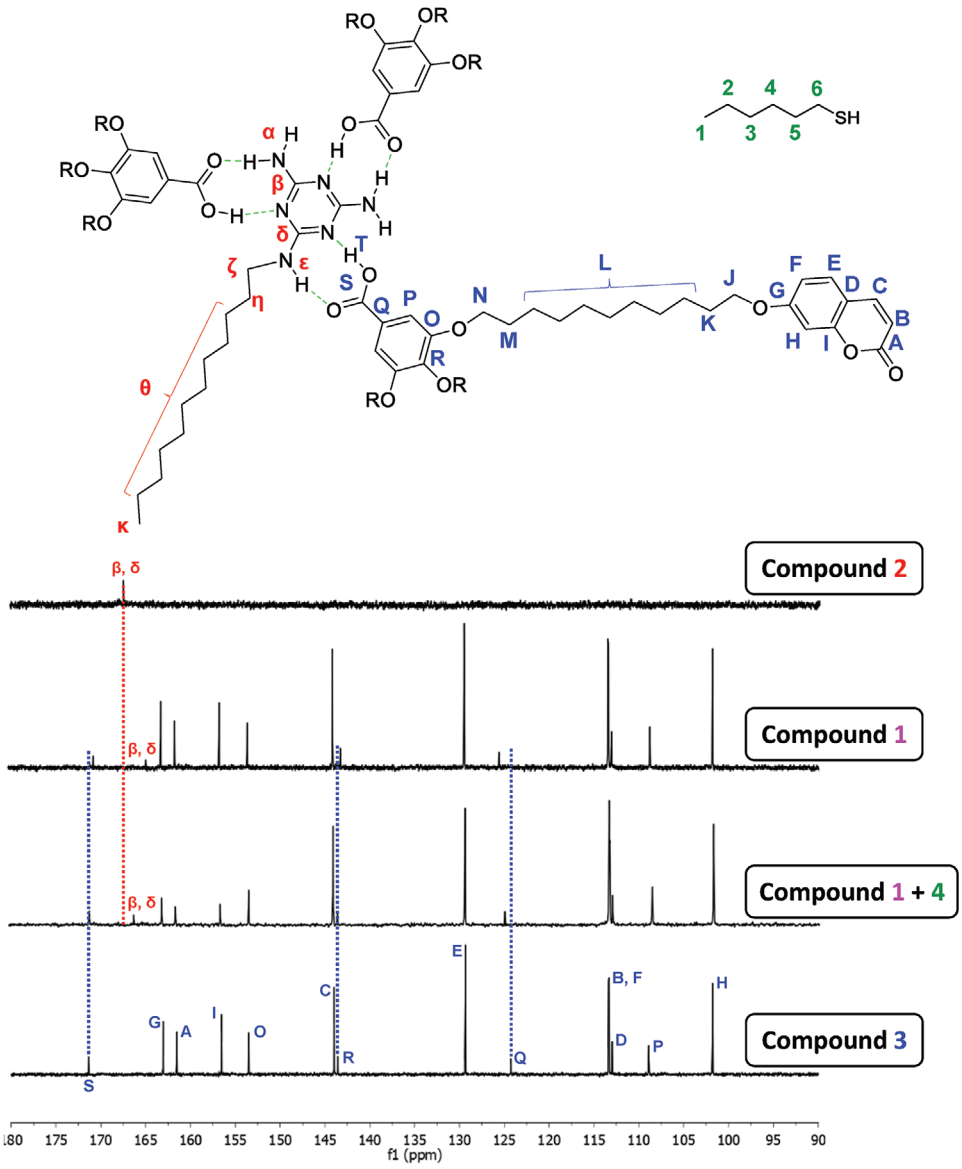

Figure 6. ^{13}C-NMR spectra (100 MHz, CD_2Cl_2) for the parent compounds (**2** and **3**) and the supramolecular structure (compound **1**) after the addition of compound **4**.

Section 3.2. includes a more detailed discussion of the NMR results. These results indicate that incubating a photo-crosslinked LB monolayer of compound **1** in a solution of 1-hexanethiol primarily induces a slight alteration in solvent polarity, leading to a weakening of the hydrogen bonds within the melamine unit. This phenomenon, coupled with the strong thiol-gold interactions, ultimately facilitates the displacement of the melamine moiety by 1-hexanethiol.

AMF images of the films after incubation in compound **4** are shown in Figure S19 (Supporting Information), ruling out the rupture of the film or the presence of 3D structures. In order to quantify the number of thiol molecules incorporated per melamine unit, electrochemical thiol desorption experiments were performed. **Figure 7** shows the cyclic voltammetry desorption experiment for compound **4** chemisorbed onto a photo-crosslinked LB monolayer of compound **1**. By using Equation (1):

$$\Gamma = \frac{\int J dV}{\nu F n} \tag{1}$$

where J is the current density, ν is the sweeping speed, F is the Faraday constant, n is the number of electrons interchanged (n = 1), V the potential and Γ the surface density. A surface coverage for compound **4** deposited onto a monolayer of compound **1** of $6.7 \cdot 10^{-11}$ mol cm^{-2} was obtained, that is, double than the number of melamine units, 3.4×10^{-11} mol cm^{-2}, indicating a deposition of ca. two molecules of the alkanethiol per melamine unit. The area of the nanopore created by the removal of the

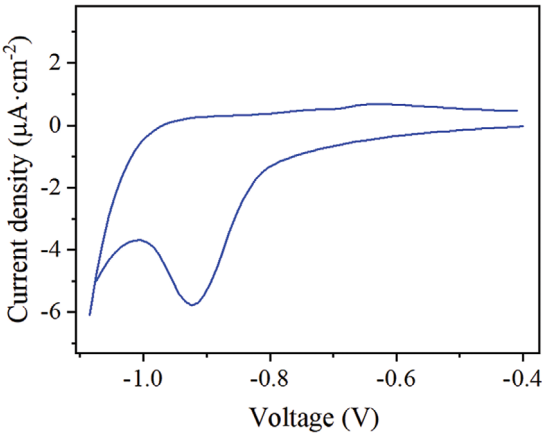

Figure 7. Cyclic voltammogram exhibiting the desorption peak of thiols for a 1-layer LB film of compound **1** incubated in a solution of compound **4**. The CV experimental conditions were: electrolyte: NaOH 0.1 M solution; reference electrode: Ag AgCl^{-1} (3 M KCl); counter electrode: Pt sheet and sweeping speed: 50 mV s^{-1}.

melamine unit has been estimated within the Spartan suit of programs as 0.37 nm^2, whilst the area of a thiol compound is ≈ 0.22 nm^2.[30] This result may tentatively be interpreted under the assumption that the dendritic units retract upon the rupture of hydrogen bonds with the melamine unit.

3. Conclusion

In this contribution, we explored the surface properties of a supramolecular compound, referred as compound **1**, which incorporates a melamine unit retained within the complex through hydrogen bonds. Our findings confirm that compound **1** forms highly ordered films at the air-water interface, readily transferable onto solid supports by the Langmuir–Blodgett method. At low surface pressures, the supramolecular compound adopts a planar orientation on the substrate, amenable to photodimerization upon exposure to UV–vis light resulting in the formation of a compact structure. Our subsequent efforts focused on demonstrating the capacity of these photo-crosslinked monolayers of compound **1** to serve as molecular templates. Importantly, the hydrogen bonds that maintain the melamine unit within the photo-crosslinked monolayer are weakened when the monolayer film is immersed in a solution containing a thiol-terminated compound. This weakening, along with the robust thiol-gold interactions, facilitates the displacement of the melamine, resulting in the chemisorption of the thiol derivative onto the underlying gold substrate. These results stand as a proof-of-concept for employing a combination of supramolecular chemistry and nanoarchitectonic tools to precisely guide the specific location of target molecules on surfaces. This approach opens pathways for diverse potential applications in sensing, electronics, thermoelectricity, and beyond.

4. Experimental Section

Synthesis of compounds **1**, **2**, and **3** was carried out following previously described methods.[25]

Langmuir and Langmuir–Blodgett (LB) films were prepared in a NIMA 702 BAM and KSV Nima KN 2003 troughs with dimensions 720 × 100 and 580 × 145 mm^2, respectively. These troughs were located in a clean room at a constant temperature of 20 °C. A Wilhelmy paper plate pressure sensor was used to measure the surface pressure (π) of the monolayers. The subphase was an aqueous (Millipore Milli-Q, resistivity 18.2 MΩ cm). 1•10^{-5} M spreading solution of compounds **1**, **2,** and **3** were freshly prepared in chloroform. Mixed isotherms of compounds **2** and **3** for the indicated ratios were prepared by mixing the two solutions and spreading the mixture on the water surface. Experimental conditions for the monolayers fabrication were: spread volume = 1.4 mL (by using a micro-syringe Hamilton–Bonaduz from Sigma–Aldrich), 30 min for solvent evaporation, compression barrier speed = 6 mm min^{-1}. Under these experimental conditions, the isotherms were highly reproducible. The direct visualization of the monolayer formation at the air/water interface was studied using a commercial mini-Brewster angle microscopy (mini-BAM); the ΔV-A measurements were carried out using a Kelvin Probe; and the UV–vis reflection experiments were recorded with a reflection spectrophotometer. BAM, Kelvin Probe, and UV–vis reflection spectrometer instruments were all provided by Nanofilm Technologie GmbH.

The monolayers at the air-water interface were transferred onto solid supports at a constant surface pressure by the vertical dipping method (dipping speed was 1 mm min^{-1}) onto cleaved mica, gold, or quartz substrates. Mica sheets were provided by Electron Microscopy Sciences Company (Cat. #71851-05, sheet size 1″ × 3″; 25 × 75 mm and thickness 0.26–0.31 mm). Each mica substrate was cut by using scissors into ≈ 1 × 1 cm^2 pieces, and subsequently were cleaved with adhesive tape prior to their use. Gold-on-glass substrates and gold-on-mica substrates were purchased from Arrandee and Georg Albert PVD – Beschichtungen, respectively. Quartz substrates were provided by Hellma (665.00 QS 45 × 12.5 mm). Quartz Crystal Microbalance (QCM) measurements were carried out using a Stanford Research System instrument and employing AT-cut, α-quartz crystals with a resonant frequency of 5 MHz having circular gold electrodes patterned on both sides. UV–vis spectra of the LB films were acquired on a Varian Cary 50 spectrophotometer, and recorded using a normal incident angle with respect to the film plane. NMR characterization was performed in a Bruker AV-300, Bruker AV-400, and Bruker AV-500. Imaging on samples was registered in ambient air conditions with a Multimode 8 from Veeco-Bruker equipped with a Nanoscope V control unit in Tapping mode. RTESPA-150 AFM probes (90–210 kHz, 1.5–10 N m^{-1} and nominal radius of 8 nm) were used and purchased from Bruker. XPS spectra were recorded on a Kratos AXIS ultra DLD spectrometer equipped with an Al Kα X-ray monochromatic source (1486.6 eV) and using 20 eV as pass energy. Binding energies were calibrated according to the C1s peak at 284.6 eV. Cyclic voltammetry (CV) experiments were carried out using an Autolab potentiostat from Eco Chemie and a standard three electrode cell, where the working electrode was a gold electrode purchased from Arrandee (bare gold or covered by a LB film of **1**) connected to the potentiostat by means of a cable terminated in a metallic crocodile clip that held the electrode.[31] The reference electrode was Ag/AgCl, KCl (3M), and the counter electrode was a *Pt* sheet.

Supporting Information

Supporting Information is available from the Wiley Online Library or from the author.

Acknowledgements

E.E., S.M., and P.C. thank PID2019-105881RB-I00 and PID2022-141433OB-I00 funded by MCIN/AEI/10.13039/501100011033 and by "ERDF A way of making Europe" as well as TED2021-131318B-I00 funded by MCIN/ AEI/10.13039/501100011033/ and Unión Europea NextGenerationEU/PRTR. J.L.S. and A.C. acknowledge PGC2018-097583-I00 and PID2021-122882NBI00 funded by MCIN/AEI/10.13039/501100011033/and by "ERDF A way of making Europe". A.C. is grateful for grant RYC2021-031154-I funded by

MICINN/AEI/FEDER/EU-NextGenerationEU. The authors also acknowledge Gobierno de Aragón–FEDER (Construyendo Europa desde Aragón) for funding the research groups Platón (E31_23R) and CLIP (E47_23R). E.E. thanks the award of a DGA fellowship from the Government of Aragon and the mobility funding for international research stays. G.Z. acknowledges funding through AlmaAttrezzature from the University of Bologna. The authors would like to acknowledge the use of the SAI (UNIZAR), CEQMA (UNIZAR–CSIC) Services, and Laboratorio de Microscopias Avanzadas-LMA (UNIZAR).

Conflict of Interest

The authors declare no conflict of interest.

Data Availability Statement

Research data are not shared.

Keywords

molecular networks, 2D molecular templates, supramolecular and interfacial chemistry

Received: December 21, 2023
Revised: March 16, 2024
Published online: April 3, 2024

[1] O. Chailapakul, R. M. Crooks, *Langmuir* **1993**, *9*, 884.
[2] J. C. Love, L. A. Estroff, J. K. Kriebel, R. G. Nuzzo, G. M. Whitesides, *Chem. Rev.* **2005**, *105*, 1103.
[3] A. Villares, D. P. Lydon, L. Porres, A. Beeby, P. J. Low, P. Cea, F. M. Royo, *J. Phys. Chem. B.* **2007**, *111*, 7201.
[4] K. Ariga, M. V. Lee, T. Mori, X.-Y. Yu, J. P. Hill, *Adv. Colloid. Interf. Sci.* **2010**, *154*, 20.
[5] K. Ariga, A. Vinu, Y. Yamauchi, Q. Ji, J. P. Hill, *Bull. Chem. Soc. Jpn.* **2011**, *85*, 1.
[6] K. E. Venta, M. B. Zanjani, X. Ye, G. Danda, C. B. Murray, J. R. Lukes, M. Drndić, *Nano Lett.* **2014**, *14*, 5358.
[7] S. Shekar, D. J. Niedzwiecki, C.-C. Chien, P. Ong, D. A. Fleischer, J. Lin, J. K. Rosenstein, M. Drndić, K. L. Shepard, *Nano Lett.* **2016**, *16*, 4483.
[8] S. C. O'Hern, M. S. H. Boutilier, J.-C. Idrobo, Y. Song, J. Kong, T. Laoui, M. Atieh, R. Karnik, *Nano Lett.* **2014**, *14*, 1234.
[9] J. A. Rodríguez-Manzo, M. Puster, A. Nicolaï, V. Meunier, M. Drndić, *ACS Nano* **2015**, *9*, 6555.
[10] J. Feng, K. Liu, M. Graf, D. Dumcenco, A. Kis, M. Di Ventra, A. Radenovic, *Nat. Mater.* **2016**, *15*, 850.
[11] M. Navarro, J. Benito, L. Paseta, I. Gascón, J. Coronas, C. Téllez, *ACS Appl. Mater. Interfaces* **2018**, *10*, 1278.
[12] G. Danda, M. Drndić, *Curr. Opin. Biotechnol.* **2019**, *55*, 124.
[13] L. Zhang, M. Jaroniec, *Chem. Soc. Rev.* **2020**, *49*, 6039.
[14] H. Chen, J. Fraser Stoddart, *Nat. Rev. Mater.* **2021**, *6*, 804.
[15] C. Tang, R. T. Ayinla, K. Wang, *J. Mater. Chem. C.* **2022**, *10*, 13717.
[16] O. N. Oliveira, L. Caseli, K. Ariga, *Chem. Rev.* **2022**, *122*, 6459.
[17] L. Dotor, J. M. García-Pinilla, S. Martín, P. Cea, *Nanoscale* **2023**, *15*, 2891.
[18] J. A. Theobald, N. S. Oxtoby, M. A. Phillips, N. R. Champness, P. H. Beton, *Nature* **2003**, *424*, 1029.
[19] J. Feng, K. Liu, M. Graf, M. Lihter, R. D. Bulushev, D. Dumcenco, D. T. L. Alexander, D. Krasnozhon, T. Vuletic, A. Kis, A. Radenovic, *Nano Lett.* **2015**, *15*, 3431.
[20] A. G. Slater, L. M. A. Perdigão, P. H. Beton, N. R. Champness, *Acc. Chem. Res.* **2014**, *47*, 3417.
[21] T. Yokoyama, S. Yokoyama, T. Kamikado, Y. Okuno, S. Mashiko, *Nature* **2001**, *413*, 619.
[22] J. Adisoejoso, K. Tahara, S. Lei, P. Szabelski, W. Rżysko, K. Inukai, M. O. Blunt, Y. Tobe, S. De Feyter, *ACS Nano* **2012**, *6*, 897.
[23] M. E. Garah, A. Ciesielski, N. Marets, V. Bulach, M. W. Hosseini, P. Samorì, *Chem. Comm.* **2014**, *50*, 12250.
[24] E. Escorihuela, A. Concellón, I. Marin, V. J. Kumar, L. Herrer, S. A. Moggach, A. Vezzoli, R. J. Nichols, P. J. Low, P. Cea, J. L. Serrano, S. Martín, *Mater. Today Chem.* **2022**, *26*, 101067.
[25] A. Concellón, A. P. H. J. Schenning, P. Romero, M. Marcos, J. L. Serrano, *Macromolecules* **2018**, *51*, 2349.
[26] H.-R. Tseng, D. Wu, N. X. Fang, X. Zhang, J. F. Stoddart, *ChemPhysChem* **2004**, *5*, 111.
[27] K. Liu, G. Li, X. Wang, F. Wang, *J. Phys. Chem. C* **2008**, *112*, 4342.
[28] G. Jayamurugan, V. Gowri, D. Hernández, S. Martín, A. González-Orive, C. Dengiz, O. Dumele, F. Pérez-Murano, J.-P. Gisselbrecht, C. Boudon, W. B. Schweizer, B. Breiten, A. D. Finke, G. Jeschke, B. Bernet, L. Ruhlmmann, P. Cea, F. Diederich, *Chem.-Eur. J.* **2016**, *22*, 10539.
[29] L. M. Ballesteros, S. Martín, G. Pera, P. A. Schauer, N. J. Kay, M. C. López, P. J. Low, R. J. Nichols, P. Cea, *Langmuir* **2011**, *27*, 3600.
[30] F. Schreiber, *Prog. Surf. Sci.* **2000**, *65*, 151.
[31] L. A. Bumm, J. J. Arnold, M. T. Cygan, T. D. Dunbar, T. P. Burgin, L. Jones, D. L. Allara, J. M. Tour, P. S. Weiss, *Science* **1996**, *271*, 1705.